Assessment of different Material Point Methods with small and large strain constitutive models

M. Xie[1] , P. Navas [2] , S. Lopez-Querol [1]

[1]Department of Civil, Environmental and Geomatic Engineering, University College London, London, UK

[2]Department of Continuum Mechanics and Structures, Universidad Politécnica de Madrid, Madrid, Spain

ABSTRACT: With increasing computational power, more and more studies currently focus on extremely large deformation in geotechnical engineering problems. The continuum-based approaches, such as the Material Point Method (MPM), are more computationally efficient than models of particles, such as the Discrete Element Method (DEM), for large deformation problems. It has been found that constitutive models based on the small strain theory are more commonly used in current research for large deformations. In these studies, objective Jaumann rates are typically used, for which the constitutive models still follow a small strain framework. Therefore, a comprehensive assessment of small strain (including Jaumann rate) and large strain formulations in conjunction with different MPMs (i.e. explicit, implicit, original and improved MPMs) is conducted in this research. Some typical large deformation geotechnical problems, such as the granular column collapse and strip footing problems, will be studied and assessed. The research outcomes will guide future researchers in choosing the appropriate constitutive frameworks (i.e. small or large strain) and the type of MPMs for their own studies.

Keywords: Material Point Method; Large strain; Constitutive model; Landslide; Strip footing

1 INTRODUCTION

Modelling large deformation geotechnical problems, such as landslides (Soga et al., 2016) and large penetration in soils (Wang et al., 2015), has become increasingly popular in recent years. The conventional mesh-based numerical methods, such as the Finite Element Method (FEM), widely used in the industry, have difficulties conducting a large deformation analysis due to the highly distorted mesh after the failure occurs. The Discrete Element Method (DEM) is suitable for large deformation problems, but its computational cost is currently not affordable for large-scale problems like landslides. The Material Point Method (MPM) has been recommended as the most favourable numerical approach for large deformation geotechnical problems due to its efficiency, similar formulation to FEM and ability for substantial deformation problems (Soga et al., 2016).

The original MPM (Sulsky et al., 1994) has a well-known cell crossing noise instability. Its improved method, Generalised Interpolation MPM (GIMPM) (Bardenhagen and Kober, 2004), has been developed to overcome this problem, although it cannot be entirely eliminated (Zhang et al., 2016). Therefore, the MPM with higher order shape function, such as B-spline MPM (BSMPM) (Steffen et al., 2008), has been developed to fully overcome the cell crossing noise. However, the GIMPM is still the most popular option in the literature. In addition to cell-crossing noise, the volumetric locking instability has drawn attention in the

MPM community. It results in unphysical stress oscillation and over-stiff kinematical behaviour (Coombs et al., 2018). However, most of the current MPM geotechnical studies lack treatment for volumetric locking. Additionally, explicit algorithms are more prevalent in the MPM than implicit ones, and the comparison between them can rarely be found in the MPM literature.

From the constitutive point of view, small strain constitutive models with an objective Jaumann rate are the most popular option in the current MPM works. However, using a small strain approach for the large deformation problem is controversial. Moreover, most of the available geotechnical research is based on basic constitutive models (e.g. Mohr-Coulomb). The performance of a more advanced constitutive model, such as the Modified Cam-Clay model, in conjunction with MPM, needs to be evaluated.

Therefore, this research aims to fill the previously mentioned research gaps by comprehensively assessing different types of constitutive models in conjunction with different versions of MPM.

2 METHODOLOGY

This research studies the explicit and implicit versions of different MPMs. We follow Wyser et al. (2020) and Guilkey and Weiss (2003) for the explicit and implicit MPM algorithms, respectively. The different shape functions adopted in the explicit or implicit algorithms distinguish between the original MPM, GIMPM and

BSMPM. The introduction of the original MPM and GIMPM shape functions can be found in Zhang et al. (2016), and the reader may refer Tran et al. (2019) for the BSMPM shape function.

These different MPMs are assessed through a granular column collapse problem with the Mohr-Coulomb model, a strip footing problem with the Modified Cam-Clay model, and the same strip footing problem with the Tresca model. For Mohr-Coulomb and Tresca models we adopt the formulation proposed by de Souza Neto et al. (2008) and the algorithm of the Modified Cam-Clay model proposed by Borja and Tamagnini (1998).

The evaluations of large strain-, Jaumann- and small strain-based constitutive models are carried out using BSMPM. The small and large strain approaches are well illustrated by de Souza Neto et al. (2008). The Jaumann approach is under the small strain framework, but its stress rate is objective. In this research, we follow the work of Wyser et al. (2020) for the Jaumann approach. An F-bar-based stabilisation method (de Souza Neto et al., 2008) is also applied to the granular column collapse problem to overcome the volumetric locking issue in MPMs. This stabilisation method is not applied to the strip footing problems for a better comparison between the Modified Cam-Clay and Tresca models.

3 NUMERICAL EXAMPLES

3.1 Granular column collapse

The first example consists of a granular column collapse experiment using different MPMs. In the original experiment, aluminium rods were used to represent the granular material (Nguyen et al., 2017). The advantage of the aluminium rods is that the in-page movement is prevented, allowing us to model this problem in a 2-D plane strain condition. Figure 1 shows the initial and final configurations of this experiment. These aluminium rods are set in a rectangle with dimensions 0.2 m in width and 0.1 m in height, against a smooth wall connected with a rough base and a removable supporting wall, as shown in Figure 1. After the sudden removal of the supporting wall, the granular flow is generated as the granular column collapses. Finally, the granular flow becomes static after 0.607 seconds (Nguyen et al., 2017).

The Mohr-Coulomb material parameters, including Young's modulus, $E = 5840$ kPa, Possion's ratio, $\nu = 0.3$, friction angle, $\phi = 21.9°$, dialation angle, $\psi = 0°$, cohesion, $c = 0$ kPa, and unite weight, $\gamma = 20.4\ kN/m^3$ are calibrated with experiments (Nguyen et al., 2017). These parameters are adopted for this numerical example. The fixed and roller boundary conditions are applied on the bottom and left side of the background mesh, respectively. The supporting wall is not modelled in this research because it was removed very quickly during the experiment (Nguyen et al., 2017). The full

gravity load is applied in the initial step and remains constant during the entire simulation (i.e. 0.607 seconds). For this problem, a square grid cell with a 6.25 mm^2 cell size is used, and thirty-six (6^2) material points are placed in each grid cell to minimise the quadrature error. A limited benefit of accuracy can be achieved by further refining the mesh. As a result, these aluminium rods are discretised into 115,200 material points. For the implicit solver, the time (i.e. 0.607 seconds) is discretised into 2428 steps. For the explicit solver, the Courant–Friedrichs–Lewy (CFL) condition with 0.98 Courant number is applied, resulting in a total of 15,381 steps.
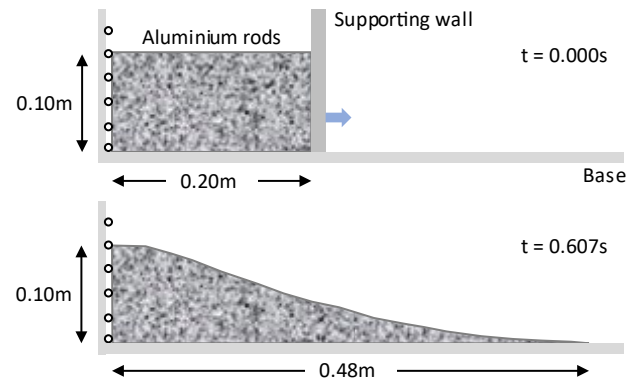

Figure 1. Initial and final configuration of the granular column collapse experiment

Figures 2(a-c) show the final configurations of the granular column collapse problem given by MPM, GIMPM, BSMPM and experiment, respectively. The right-hand side of Figure 2 shows the vertical stress results given by the implicit solver, and the left-hand side shows the results given by the explicit solver. As shown in Figure 2, the MPMs with no stabilisation have highly oscillated stress fields due to the volumetric locking. In contrast, the F-bar-based stabilisation has solved this non-physical stress oscillation.

The volumetric locking is more severe in the MPM and GIMPM than in the BSMPM. As shown in Figure 2, the stress contour given by BSMPM with no stabilisation has not been strongly smeared compared with the contours given by MPM and GIMPM. Also, the crests of the granular flow given by MPM and GIMPM with no stabilisation have poor agreements with the experiment, as shown in Figures 2(a) and (b). On the contrary, the BSMPM with no stabilisation has an excellent agreement on the crest of the granular flow. The least volumetric locking is obtained in BSMPM because this method has a higher order shape function than the MPM and GIMPM. However, the highly oscillated stresses result in a significantly overestimated runout distance for all MPMs with no stabilisation, as shown in Figure 2. A
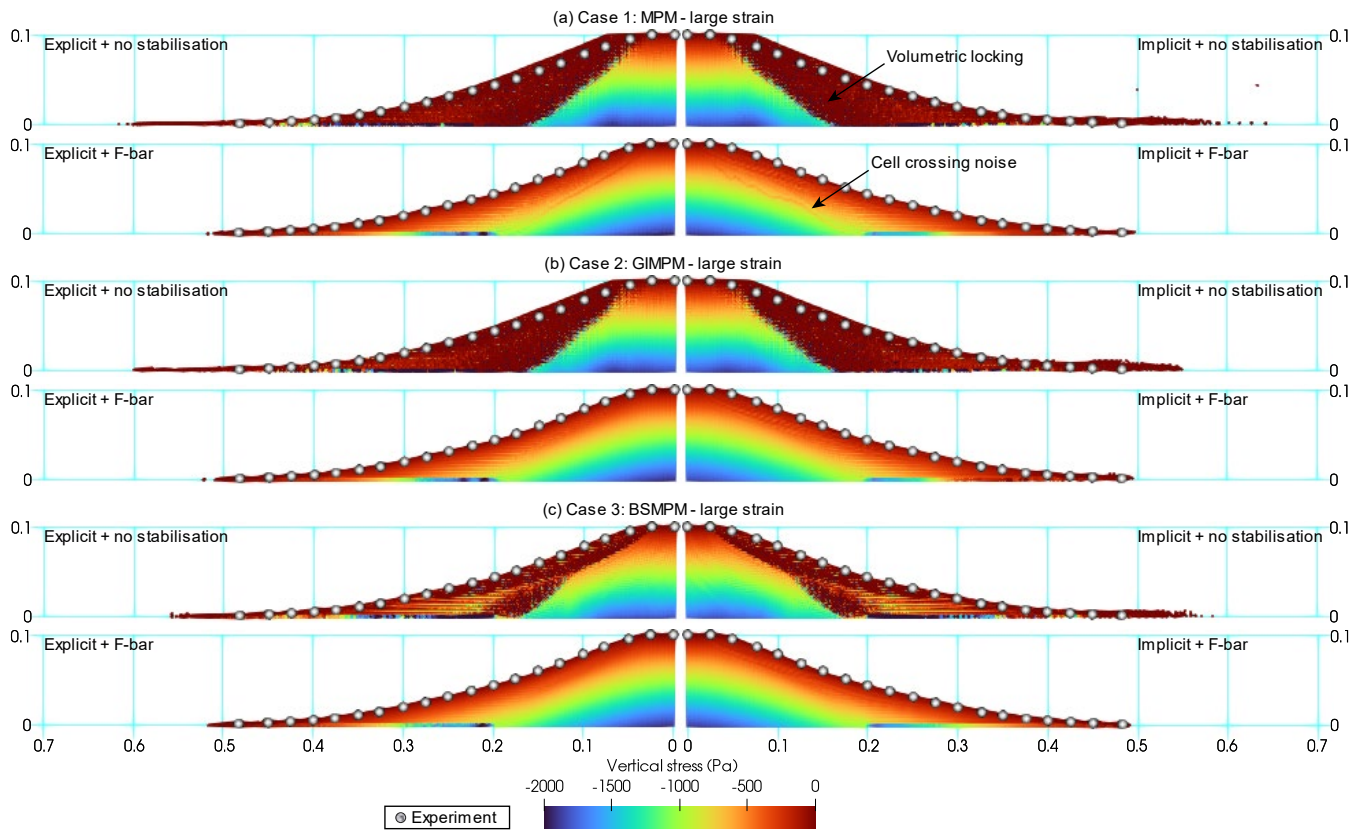
Figure 2. Final configuration of granular column collapse experiment with the simulation results given by different explicit and implicit MPMs with large strain Mohr-Coulomb model: (a) MPM; (b) GIMPM; (c) BSMPM

better estimation of runout distance can be observed in the case of F-bar-based stabilisation.

After removing volumetric locking, the BSMPM yields the smoothest stress contour, as shown in Figure 2(c). A relatively strong noise can still be observed in the case of MPM with the F-bar-based method. This noise is the well-known cell crossing instability in the original MPM. Figure 2(b) shows that the cell crossing noise has been significantly controlled in the GIMPM. However, there are still some stress instabilities in the

GIMPM compared with the BSMPM because GIMPM cannot fully remove the cell crossing noise (Zhang et al., 2016), which results in a slightly over-predicted runout distance.

As shown in Figure 2, the simulation result given by implicit BSMPM with the F-bar-based method has the highest agreement with the experiment amount of the others. The explicit solver results in a longer runout distance than the implicit one, as seen in Figure 2 and Figure 3(a).

Figure 3(a) compares the evolutions of maximum runout distance given by large strain, small strain and Jaumann approaches. For this granular column collapse problem, the kinematical difference between the small and large strain constitutive models is insignificant, as depicted in Figure 3(a). However, the evolutions of the internal variable (the accumulated plastic strain in this case) are significantly different between the small and large strain approaches, as shown in Figure 3(b). The
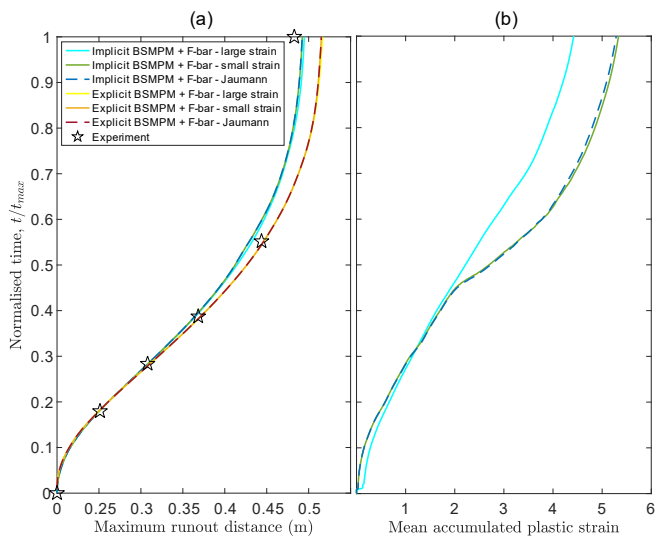

Figure 3. Results of granular column collapse problem: (a) Evolution of maximum runout distance; (b) Evolution of internal variable
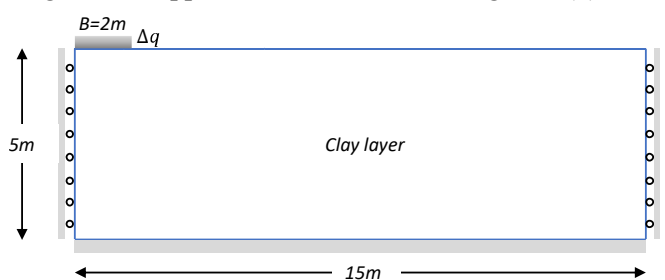

Figure 4. Geometry and boundary conditions of the flexible strip footing problem
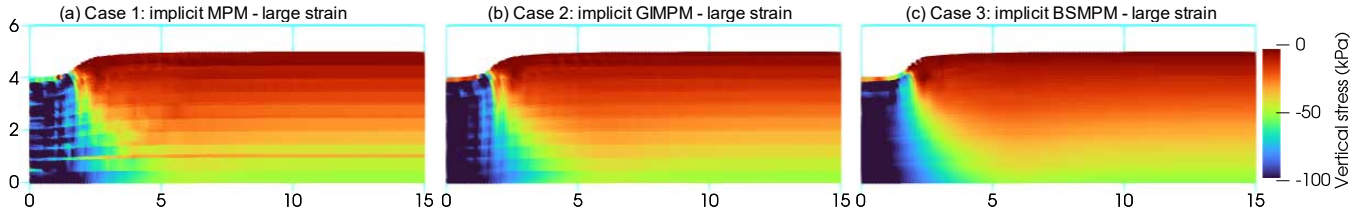
Figure 5. Simulations of Modified Cam-Clay strip footing by large strain implicit MPMs: (a) MPM; (b) GIMPM; (c) BSMPM

accumulated plastic strain develops faster in the small strain approach. The small strain and the Jaumann approaches have similar evolution of accumulated plastic strain. However, when the deformation goes large, the curve given by the Jaumann approach slightly diverges from the curve given by the small strain approach, see Figure 3(b).

Moreover, globally, the internal variable controls the hardening behaviour of a constitutive model. In the case of a model enhanced with hardening behaviour, a large kinematical variation can be expected between the small and large strain approaches.

3.2 Modified Cam-Clay flexible strip footing

In this research, we follow the same Modified Cam-Clay strip footing problem previously studied by Borja and Tamagnini (1998) using FEM. In this problem, a uniformly distributed load, $\Delta q = 90 kPa$, representing a flexible strip footing, is applied in a homogeneous soft clay layer modelled in 2-D plane strain condition, as shown in Figure 4. The half-width, B, of this footing is 2.0 m, and the width and thickness of the underneath clay layer are 15.0 m and 5.0 m, respectively. The clay layer has a fixed boundary condition on its bottom and rollers on its sides.

The material parameters for this clay layer are: elastic compressibility, $\hat{\kappa} = 0.018$, plastic compressibility, $\hat{\lambda} = 0.130$, constant elastic shear modulus, $\mu_0 = 5400\ kPa$, the slope of critical state line, $M = 1.05$, a constant coefficient, $\alpha = 0$, and the unit weight, $\gamma = 10\ kN/m^3$. Before applying the gravity load, the reference pressure, p_0, and the preconsolidation pressure, p_c, are set to be 20 kPa. The initial elastic volumetric strain, ε_{v0}^e, is set to zero. To generate the initial stress and the preconsolidation pressure, the gravity load is gradually applied to the clay layer in 20 steps and 100 seconds for the implicit static and the explicit solver, respectively. After that, the uniformly distributed load is incrementally applied in 50 steps and 100

seconds for the implicit static and explicit solvers, respectively. According to the investigation, applying the load in 100 seconds is slow enough to represent the quasi-static behaviour for this strip footing problem. The square grid cell with a 0.25 m² cell size is used in this research, which is consistent with the smallest FEM grid cell in the research conducted by Borja and Tamagnini (1998). For this numerical example, a configuration of sixteen (4^2) per grid cell is sufficient to control the quadrature error. The simulation results are examined as not sensitive to the mesh density for this Modified Cam-Clay strip footing problem.
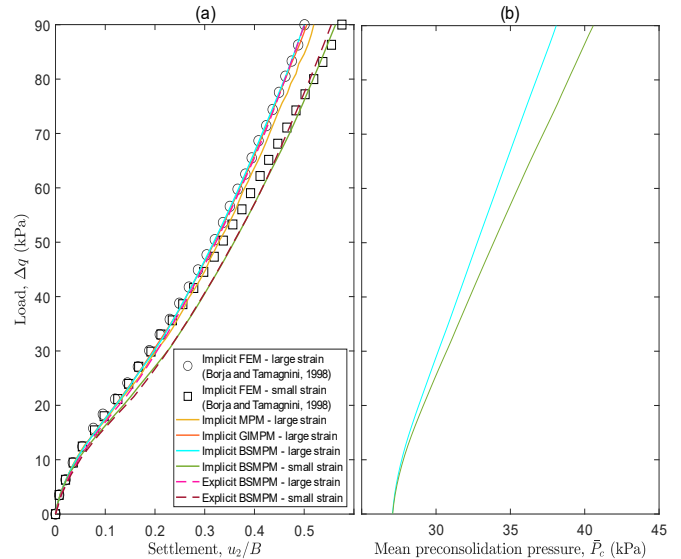

Figure 6. Results of Modified Cam-Clay strip footing: (a) Load-settlement curve; (b) Evolution of internal variable

Figures 5(a-c) show the vertical stress result of the Modified Cam-Clay strip footing problem given by implicit MPM, GIMPM and BSMPM, respectively. The explicit solvers produce very similar contour maps, and therefore, they are not presented in this paper. No volumetric locking phenomenon is observed in the Modified
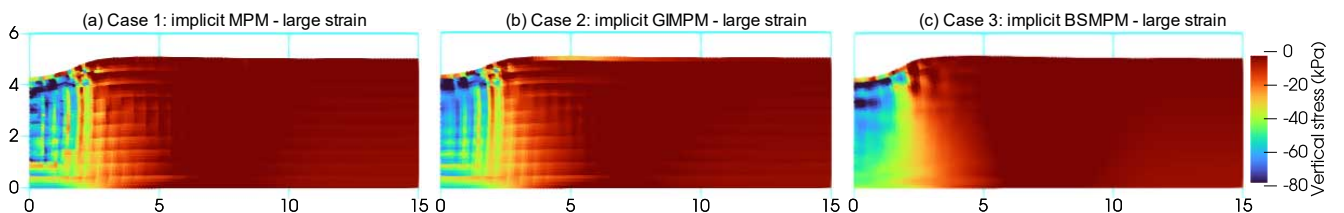

Figure 7. Simulations of Tresca strip footing by large strain implicit MPMs: (a) MPM; (b) GIMPM; (c) BSMPM

Cam-Clay constitutive model results, as shown in Figures 5(a-c). The closely matched load-settlement curves given by GIMPM and BSMPM (see Figure 6(a)) is also a evidence of no volumetric locking in the Modified Cam-Clay model. However, the non-physical stress oscillations due to cell crossing noise are observed in the results given by the original MPM and GIMPM, as shown in Figures 5(a) and (b). As expected, the GIMPM produces less cell crossing noise than the original MPM. Moreover, the BSMPM has the most stable stress field since the BSMPM does not have cell crossing noise.

The implicit MPM and GIMPM only work on the current mesh density. They cannot achieve a converged solution once the background mesh has been refined, as the material points cross the cell boundaries more frequently in a refined background mesh. However, the implicit BSMPM with the Modified Cam-Clay model has no convergence issue for a refined background mesh. On the contrary, the explicit solvers are stable as long as the time step is smaller than the one given by the CFL condition. The cell crossing noises produced by GIMPM have not significantly altered the kinematics for this numerical example. As shown in Figure 6(a), the load-settlement curve given by GIMPM has an excellent agreement with the FEM (Borja and Tamagnini, 1998) and BSMPM. However, the strong cell crossing noise in the original MPM causes the load-settlement curve to significantly divert from the FEM (Borja and Tamagnini, 1998) and BSMPM, as shown in Figure 6(a).

The Jaumann approach cannot be applied to this Modified Cam-Clay constitutive model since it is written in a rate-independent formulation (Borja and Tamagnini, 1998). The results given by small and large strain constitutive models are significantly different for this Modified Cam-Clay strip footing problem. As shown in Figure 6(a), the small strain constitutive model overestimates the settlement of the footing in the large deformation range. This finding is consistent with the FEM study (Borja and Tamagnini, 1998). Same to the Mohr-Coulomb model, the evolutions of the internal variable (preconsolidation pressure in this case) are also different between the small and large strain constitutive models. As shown in Figure 6(b), the evolution of the preconsolidation pressure in the small strain Modified Cam-Clay model is faster than the speed in the large strain model.

3.3 Tresca flexible strip footing

In the third numerical example, we study the same flexible strip footing shown in Figure 4 but now using the Tresca model with isotropic hardening. Young's modulus, $E = 1000$ kPa, and Poisson's ratio, $\nu = 0.33$, are adopted as the elastic material parameters for this Tresca clay layer. We allow isotropic hardening for this model to represent the preconsolidation behaviour of

the clay. The initial cohesion, $c_0 = 10$ kPa, and the ultimate cohesion, $c_{ult} = 15$ kPa, are assumed. In this constitutive model, the accumulated plastic strain, $\bar{\varepsilon}^p$, controls its hardening behaviour. We link the current cohesion, c, with c_0, c_{ult} and $\bar{\varepsilon}^p$ using Equation 1 proposed by Bui and Nguyen (2021)

$$c = c_{ult} + (c_0 - c_{ult})e^{-\eta \cdot \bar{\varepsilon}^p} \qquad (1)$$

where $\eta = 5$ is a hardening coefficient. In this problem, the uniformly distributed load, $\Delta q = 70 kPa$, is applied in 100 steps and 100 seconds for the implicit static solver and explicit solver, respectively.

Figures 7(a-c) show the vertical stress given by MPM, GIMPM and BSMPM. The stress oscillation due to volumetric locking can be observed in Figures 7(a-c). Also, the load-settlement curves given by MPM and GIMPM are stiffer than BSMPM due to more serious volumetric locking issues, as shown in Figure 8(a). As illustrated in the previous example, these volumetric locking phenomena have not been observed with the Modified Cam-Clay model.

In this numerical problem, the Jaumann approach results in a similar load-settlement curve compared to the small strain model, as shown in Figure 8(a). Also, the evolutions of the internal variable (the accumulated plastic strain in this case) are very similar in the Jaumann and small strain approaches, as shown in Figure 8(b). Identical to the Modified Cam-Clay model, the small strain Tresca model also overestimates the settlement when a large deformation occurs. Additionally, the evolution of the internal variable is also faster in the small strain model.

Finally, the implicit and explicit solvers yield very similar results for these two strip footing problems, as shown in Figure 6(a) and Figure 8(a). However, the explicit solver needs significantly larger computational time than the implicit solver to represent a quasi-static response.
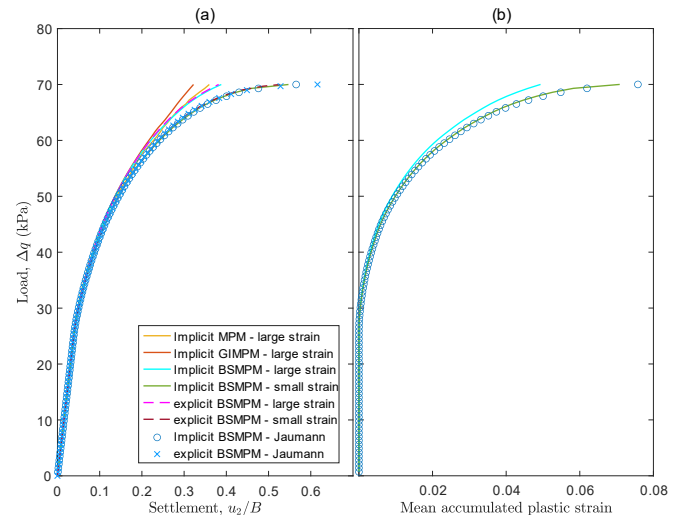

Figure 8. Results of Tresca strip footing: (a) Load-settlement curve; (b) Evolution of internal variable

4 CONCLUSIONS

The original MPM experiences severe cell-crossing noise in these numerical examples, which is significantly reduced by GIMPM. The latter results in an acceptable performance in conjunction with a basic constitutive model (e.g. Mohr-Coulomb model). However, in more advanced constitutive models such as the Modified Cam-Clay model, the implicit MPM and GIMPM have convergency issues due to the cell crossing noise. On the contrary, the implicit BSMPM fully overcomes cell-crossing noise, which is more robust and can handle more complex constitutive models.

In addition to cell-crossing noise, volumetric locking is another source of instability in MPMs. Volumetric locking is found as a constitutive model-related issue, and it can be more pronounced in MPMs. For example, MPMs that use the Mohr-Coulomb or Tresca models are more prone to volumetric locking, while MPMs that use the Modified Cam-Clay model are free of this issue. For the granular column collapse problem, volumetric locking not only results in an over-stiff behaviour at the crest but also produces an overestimated runout distance. Secondly, BSMPM shows significantly less volumetric locking problem.

The evolutions of internal variables, such as accumulated plastic strain and preconsolidation pressure, can significantly differ between the small and large strain approaches in MPM simulations. However, a limited difference is found between the small strain and the Jaumann approaches. The kinematical difference between the small and large strain methods is not obvious for problems with no hardening behaviour, such as the granular column collapse problem. However, the difference between the small and large strain approaches is significant for constitutive models with hardening behaviour, such as the Modified Cam-Clay model. In summary, the large strain approach is more accurate mathematically than the small strain approaches (including Jaumann), although we can have comparable results in several MPM simulations, especially for problems without hardening behaviour. If we consider soil models with a palpable hardening behaviour, it is not acceptable the employment of small strain approaches if the final deformation of the geo-structure is big.

5 ACKNOWLEDGEMENTS

6 REFERENCES

Bardenhagen, S.G. and Kober, E.M. 2004. The Generalized Interpolation Material Point Method, *The Generalized Interpolation Material Point Method* **5(6)**, 477–496.

Borja, R.I. and Tamagnini, C. 1998. Cam-Clay plasticity part III: Extension of the infinitesimal model to include finite strains, *Computer Methods in Applied Mechanics and Engineering* **155(1–2)**, 73–95.

Bui, H.H. and Nguyen, G.D. 2021. Smoothed particle hydrodynamics (SPH) and its applications in geomechanics: From solid fracture to granular behaviour and multiphase flows in porous media, *Computers and Geotechnics* **138**, 104315.

Coombs, W.M., Charlton, T.J., Cortis, M. et al. 2018. Overcoming volumetric locking in material point methods, *Computer Methods in Applied Mechanics and Engineering* **333**, 1–21.

Guilkey, J.E. and Weiss, J.A. 2003. Implicit time integration for the material point method: Quantitative and algorithmic comparisons with the finite element method, *International Journal for Numerical Methods in Engineering* **57(9)**, 1323–1338.

Nguyen, Cuong T., Nguyen, Chi T., Bui, H.H. et al. 2017. A new SPH-based approach to simulation of granular flows using viscous damping and stress regularisation, *Landslides* **14(1)**, 69–81.

Soga, K., Alonso, E., Yerro, A. et al. 2016. Trends in large-deformation analysis of landslide mass movements with particular emphasis on the material point method, *Géotechnique* **66(3)**, 248–273.

de Souza Neto, E.A., Perić, D. and Owen, D.R.J. 2008. *Computational Methods for Plasticity*, Wiley, Chichester, UK.

Steffen, M., Kirby, R.M. and Berzins, M. 2008. Analysis and reduction of quadrature errors in the material point method (MPM), *International Journal for Numerical Methods in Engineering* **76(6)**, 922–948.

Sulsky, D., Chen, Z. and Schreyer, H.L. 1994. A particle method for history-dependent materials, *Computer Methods in Applied Mechanics and Engineering* **118(1–2)**, 179–196.

Tran, Q.-A., Wobbes, E., Sołowski, W. et al. 2019. Moving least squares reconstruction for B-spline Material Point Method. *Proceedings of the Second International Conference on the Material Point Method for Modelling Soil-Water-Structure Interaction*, 35–41. University of Cambridge, Cambridge, UK.

Wang, D., Bienen, B., Nazem, M. et al. 2015. Large deformation finite element analyses in geotechnical engineering, *Computers and Geotechnics* **65**, 104–114.

Wyser, E., Alkhimenkov, Y., Jaboyedoff, M. et al. 2020. A fast and efficient MATLAB-based MPM solver: fMPMM-solver v1.1, *Geoscientific Model Development* **13(12)**, 6265–6284.

Zhang, X., Chen, Z. and Liu, Y. 2016. *The Material Point Method: A Continuum-Based Particle Method for Extreme Loading Cases*, Elsevier, Amsterdam, Netherlands.